Chinese Journal of Chemical Engineering 27 (2019) 3036–3042

Contents lists available at ScienceDirect

Chinese Journal of Chemical Engineering

journal homepage: www.elsevier.com/locate/CJChE

Article

Controlling pore structures of Pd-doped organosilica membranes by calcination atmosphere for gas separation☆

Yibin Wei, Hengfei Zhang, Jiaojiao Lei, Huating Song, Hong Qi *

State Key Laboratory of Material-Oriented Chemical Engineering, Membrane Science and Technology Research Center, Nanjing Tech University, Nanjing 210009, China

ARTICLE INFO

Article history:
Received 24 December 2018
Received in revised form 13 March 2019
Accepted 13 March 2019
Available online 4 April 2019

Keywords:
Pd doping
Organosilica membrane
Calcination atmosphere
Gas separation

ABSTRACT

Pd-doped organosilica membranes were prepared by controlling calcination atmospheres (*i.e.* POS-Air, POS-N_2, POS-H_2, POS-H_2/N_2) to tailor their networks for improving their gas separation performance. This study shows that Pd (II) could be only maintained under non-reductive calcination atmosphere, while inert and reducing calcination atmosphere is more beneficial to maintain organosilica moieties in POS networks. POS-H_2/N_2 membrane showed the optimal H_2 separation performance that its permselectivities for H_2/CO_2, H_2/N_2, H_2/CH_4 and H_2/SF_6 are 15.0, 96.7, 173.0 and 3400.0, respectively. Moreover, it is found that H_2 molecules pass through the four membranes based on activated diffusion, while CO_2 molecules permeation through POS-N_2 and POS-Air membrane is dominated by surface diffusion. This work may provide insight into the understanding of the calcination atmosphere effect on gas separation performance of metal-doped organosilica membranes.

1. Introduction

Over recent decades membrane-based technologies have been proven to be effective solutions to critical challenges that human beings are facing today, such as the efficient production of fuels, chemicals, renewable energy, and drinking water; as well as advanced environmental remediation and climate change mitigation [1–3]. Inorganic ceramic membranes exhibit excellent mechanical, thermal and chemical stability, which allow them to be promising for gas separation. Among the ceramic membranes, microporous silica-based membranes have drawn a great deal of attention for molecular sieving applications owing to their tunable pore size [4].

The first gas separation silica membrane was prepared by Uhlhorn *et al.* in 1989 [5]. Their membranes were asymmetric with a structure consisting of three layers including a macroporous α-Al_2O_3 support layer, a mesoporous γ-Al_2O_3 intermediate layer and a microporous silica separation layer, exhibiting excellent CO_2/CH_4 separation performance. A few years later, de Vos *et al.* [6] reported an ultra-thin microporous silica membrane with superior hydrogen separation performance (H_2 permeance of 5×10^{-7} mol·m^{-2}·s^{-1}·Pa^{-1} and H_2/CO_2 permselectivity of 71), which signifies an important step toward industrial application of H_2/CO_2 separation. However, many follow-up studies pointed out that microporous silica materials are unstable in a steam environment [7]. Si—O—Si groups in silica network can decompose into mobile silanol encountering H_2O at high temperature, leading to the formation of non-selective pores [8]. Therefore, hydrothermal stability is another critical criterion in addition to permeability and permselectivity, and the poor hydrothermal stability of silica membranes limits its real industrial application in H_2/CO_2 separation.

In 2007, Castricum *et al.* [9] prepared an organic–inorganic hybrid silica membrane derived from the precursor 1, 2-bis(triethoxysilyl)ethane (BTESE) and the co-reactant methyltriethoxysilane (MTES), for n-butanol dehydration *via* pervaporation process. It is worth noting that the membrane showed not only the excellent separation performance (water flux of 10 kg·m^{-2}·h^{-1} and the separation factor ~1000) but also unprecedented hydrothermal stability. In a moderate steam atmosphere at 150 °C, 4% water flux decline of the membrane was found per month, and the water flux kept up to 5 kg·m^{-2}·h^{-1} after running 500 days. Inspired by this, Tsuru's group [10] successfully prepared BTESE membranes used for gas separation for the first time, which can achieve ~10^{-5} mol·m^{-2}·s^{-1}·Pa^{-1} level in H_2 permeance under hydrothermal conditions. The hydrothermal stability of amorphous silica-based membranes with an organic bridging group between two Si atoms (also known as organosilica membranes) was then extensively studied proving their enhanced hydrothermal stability when compared with that of pure inorganic silica membranes and methylated silica membranes [11–16].

Among organosilica membranes, BTESE derived membranes with the ethylene-bridged network have been considered the most promising for H_2/CO_2 separation under hydrothermal conditions [17]. The sol–gel method is commonly used to prepare silica-based membranes and the preparation procedure usually consists of three steps including synthesis of sol, coating (*e.g.* spray and dip) and calcination (Fig. 1) [18]. The sol–gel chemistry controlled by synthesis parameters can ultimately affect the

☆ Supported by the National Natural Science Foundation of China (21276123, 21490581), the National High Technology Research and Development Program of China (2012AA03A606) and the "Summit of the Six Top Talents" Program of Jiangsu Province.

* Corresponding author.
E-mail address: hqi@njtech.edu.cn (H. Qi).

https://doi.org/10.1016/j.cjche.2019.03.021
1004-9541/

structure and properties of the membranes [19]. The sol needs to be carefully tuned prior to coating for avoiding sol permeation into the substrates. Calcination is the last step in forming the microporous structure and removing water and organic impurities [20]. It should be noted that the organic chains could be pyrolyzed under harsh calcination conditions and the calcination process of the preparation of silica-based membranes should be carefully selected [21].

Although pure BTESE membranes exhibit good H_2 permeability, its low H_2/CO_2 permselectivity still remains challenging to meet the requirement of industrial application [22–24]. Doping metals such as Mg, Zr, Co, Pd, Nb and *etc.*, into silica networks has been regarded as an effective strategy to improve hydrothermal stability and H_2/CO_2 permselectivity of silica network [4,25–30]. However, the trade-off between permeability, permselectivity and hydrothermal stability still exists in the reported metal-doped organosilica membranes. The introduction of metals doubtlessly improves the complexity of the organosilica networks and leads to synergetic gas separation results [31]. More experimental and theoretical efforts are required to elucidate these new phenomena for designing and developing desirable membranes. Our recent studies [32,33] confirmed that incorporating palladium (Pd) into BTESE-derived organosilica network could greatly improve the H_2 permeability of the membrane due to the high attraction of Pd to hydrogen atoms. Both metal dopant and organosilica network of a membrane are influenced by calcination process, but this effect on Pd-doped organosilica (POS) membrane lacks investigation.

Therefore, in this study, we investigate the effect of four typical calcination atmospheres on the gas separation performance of the Pd-doped organosilica (POS) membranes. As illustrated in Fig. 1, a POS sol, which has to be suitable for dip coating onto a substrate, was synthesized and characterized. Followed by a coating process, four POS membranes were fabricated by calcination in air, N_2, H_2 and H_2/N_2 atmospheres, respectively. X-ray diffractometry (XRD), transmission electron microscopy (TEM), Fourier transform infrared (FTIR) spectroscopy and N_2 sorption measurements are used to investigate the chemical state and microstructure of the four membranes. Single-gas permeation of the four membranes was evaluated under different temperatures. H_2 and CO_2 transport mechanisms of the four POS membranes were explored and discussed.

2. Experimental

2.1. Materials

1, 2-Bis(triethoxysilyl)ethane (BTESE, 97% purity) from ABCR GmbH was used as the precursor. Palladium chloride ($PdCl_2$, purity >98%) was purchased from Meryer. Ethanol anhydrous (EtOH) and acetylacetone (AcAc purity >99%) were purchased from Shanghai LingFeng Chemical Reagent Co., Ltd. Concentrated hydrochloric acid (36 wt%–38 wt% aqueous solution) was purchased from Liyang Dongfang Chemical Reagent Co., Ltd. All chemicals were used as received without further purification.

2.2. Preparation of sols, gels and membranes

The details of the preparation procedure for the Pd-doped organosilica (POS) sols could be found in our previous studies [32,33]. The composition of the obtained POS sol is BTESE:Pd:EtOH:H_2O:H^+ = 1:0.22:94.71:55.55:0.68 (molar ratio). The molar ratio of Pd:Si = 0.11:1. POS gels were prepared by drying the corresponding sols for 24 h in Petri dishes at ambient temperature. The obtained gels were then ground into fine powders and calcined under different atmospheres. Four calcination atmospheres, *i.e.* air, N_2, H_2, and H_2/N_2 (n (H_2):n (N_2) = 2:3) were investigated, and the calcined powders were marked as POS-Air, POS-N_2, POS-H_2 and POS-H_2/N_2, accordingly, for further characterization. The calcination procedure includes a heating process with a rate of 0.5 °C·min^{-1}, dwelling for 3 h at 400 °C and a cooling process with a rate of 0.5 °C·min^{-1}.

To prepare POS membranes, a POS sol was first diluted (Si concentration of 0.17 mol·L^{-1}) and then dip-coated onto home-made mesoporous γ-Al_2O_3 disc substrate with pore diameters of 3–5 nm in a clean room condition [14]. The dip-coating process was conducted using an automatic coating machine (Pervatech B.V., Netherland) at a withdraw speed of 1.2 cm·s^{-1}. The coated membranes were first dried at 40 °C for 3 h in an oven. The POS-N_2, POS-H_2, POS-H_2/N_2 and POS-Air membranes were finally prepared based on the same calcination conditions as those used for the preparation of above-mentioned POS powders.

2.3. Characterization of powders and membranes

Particle size distributions of the freshly prepared sols were measured by a nanosizer (Zetatrac, NPA152, Microtrac Inc.) at 30 °C. The particle size distribution and mean particle size of sols were calculated by the Microtrac software. Thermal behaviors of the gel powders were evaluated by thermogravimetric analysis (TGA, STA-449-F3, Netzsch) with a heating rate of 10 °C·min^{-1} from 20 °C to 800 °C under N_2 or air atmosphere. The crystalline structure of POS powder samples was analyzed by X-ray diffractometry (XRD, D8-Advance, Bruker) using a Cu K_α radiation at 40 kV and 15 mA. Fourier transform infrared (FTIR) spectra were used to determine the chemical composition of the POS powders by a Thermo NICOLET 8700. A transmission electron microscope (TEM, JEM-200CX, JEOL) was used to image and observe morphological characteristics of the POS structures. N_2 adsorption–desorption isotherms at 77 K were conducted using Micromeritics ASAP 2020 to evaluate microstructures of the POS powders. The powders were degassed under vacuum at 473 K for 12 h prior to measurements. Pore size distributions of the POS powders could be estimated *via* the N_2 adsorption–desorption isotherms based on cylindrical pore model.

2.4. Gas permeation measurement

Single-gas permeation of as-prepared POS membranes was measured at 200 °C under a transmembrane pressure of 0.3 MPa using a

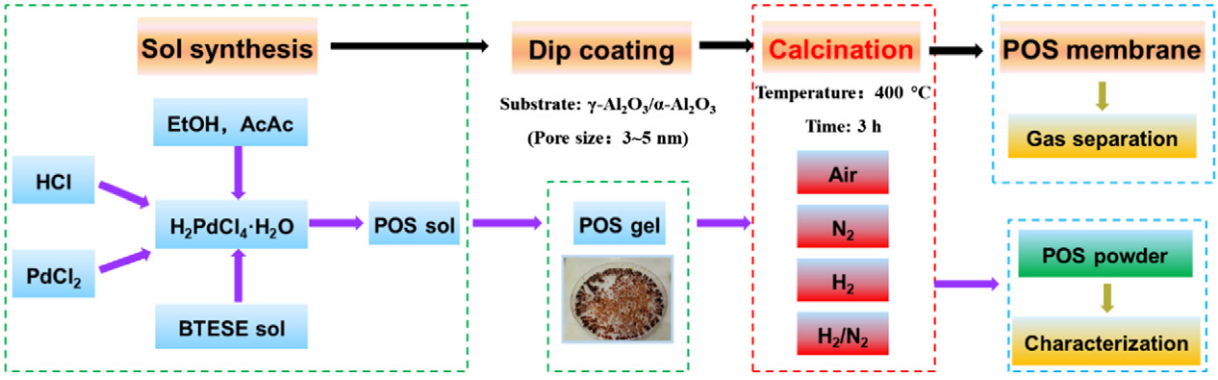

Fig. 1. Schematic illustration for the preparation process of POS powders and membranes.

dead-end mode apparatus. The membranes were tested using single gases with different kinetic diameters (d_k) [He (0.255 nm), H_2 (0.289 nm), CO_2 (0.33 nm), N_2 (0.364 nm), CH_4 (0.38 nm), to SF_6 (0.55 nm)]. The gas permselectivity, also known as ideal selectivity, was equal to the permeance ratio between two gases.

3. Results and Discussion

3.1. Sol–gel of POS

Fig. 2 shows the appearance and particle size distribution of the as-prepared POS sol. It is observed that the sol is homogeneous in reddish brown color. We also found the sol could be stored at −16 °C for 14 months without any agglomeration, which indicates that the as-prepared sol is extremely stable. Because the γ-Al_2O_3 support layer has a pore size of 3–5 nm, to avoid sol permeating into substrates, sols with mean particle sizes larger than 5 nm and uniform particle size distribution are desirable for coating. The sol has a narrow unimodal particle size distribution with 5.62–11.70 nm and a mean particle size of 7.53 nm, which could be selected for membrane preparation.

Fig. 3 describes the thermal evolutions of the as-prepared POS gel under N_2 and air atmosphere heating from 20 °C to 800 °C. The mass loss of POS gel measured under N_2 and air atmosphere showed a similar tendency that a three-stage mass loss could be clearly observed from the TG curves. In the first stage, about 20% of POS gel mass was lost when measured under air or N_2 atmosphere between 80 and 130 °C, which was caused by the loss of physically adsorbed water and solvent. For POS gel measured under N_2 atmosphere, 4% and 7% of mass loss were found in the temperature ranges of 200–250 °C and 250–800 °C, respectively. This might be attributed to the dehydroxylation and decomposition of the organic moieties, respectively [21]. Notably, an exothermic peak was observed in differential scanning calorimetry (DSC) for the POS gel measured under air atmosphere at 406 °C, and the mass loss for the temperature range of 130–500 °C is 9%. We attribute this to thermal oxidation decomposition, because ≡Si—C—C—Si≡ in the POS matrix could be decomposed under high-temperature oxidation condition. Therefore, to maintain the organic moiety in the network, the calcination temperature of POS membranes should be below 400 °C, which agrees with the other report [34]. It can also be deduced that the calcination atmosphere has a significant influence on the POS microstructures and the resultant gas separation performance.

3.2. Characterization of POS membranes

It is commonly believed that the as-prepared POS powders could be characterized for reflecting the properties of the corresponding POS layer of as-prepared membranes [35]. Fig. 4 shows XRD patterns of the POS powders calcined under air, N_2, H_2 and H_2/N_2 atmosphere. As can be seen from the optical photos of the POS powders (inset of Fig. 4), the colors of the calcined POS powders differ from the original color of POS gel powders, and the colors of POS powders calcined by

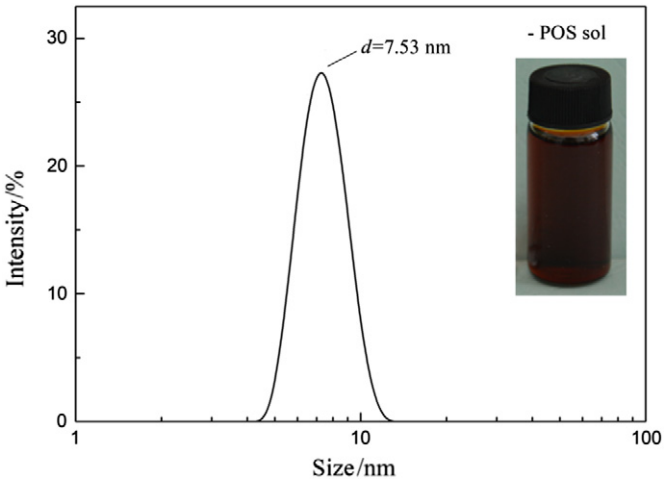

Fig. 2. Particle size distribution of the as-prepared POS sol.

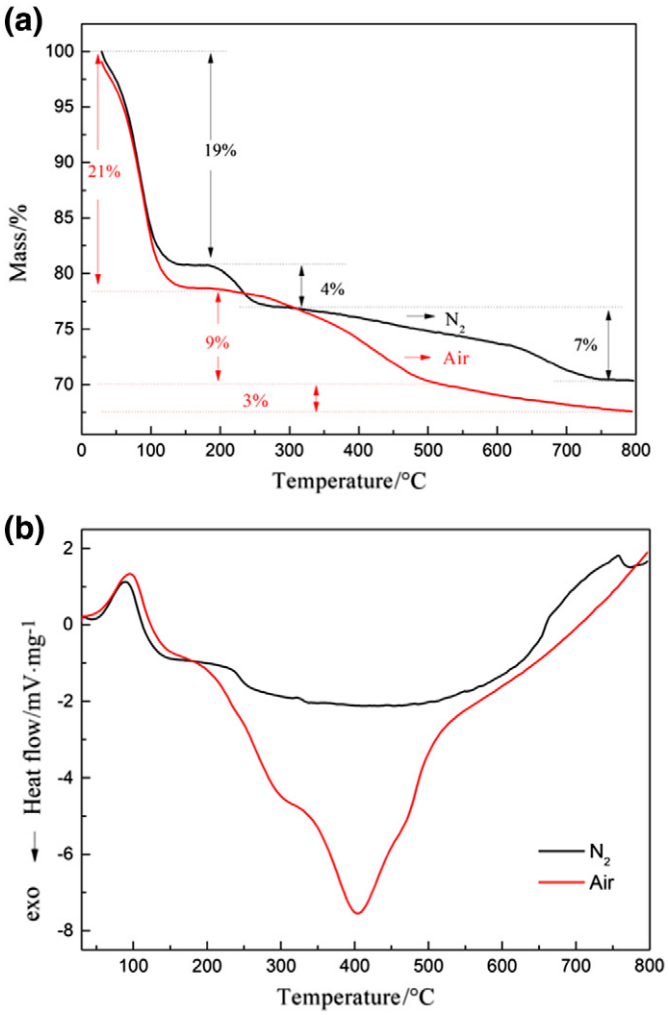

Fig. 3. (a) Thermogravimetric and (b) differential scanning calorimeter curves of the POS gels under air and N_2 atmosphere.

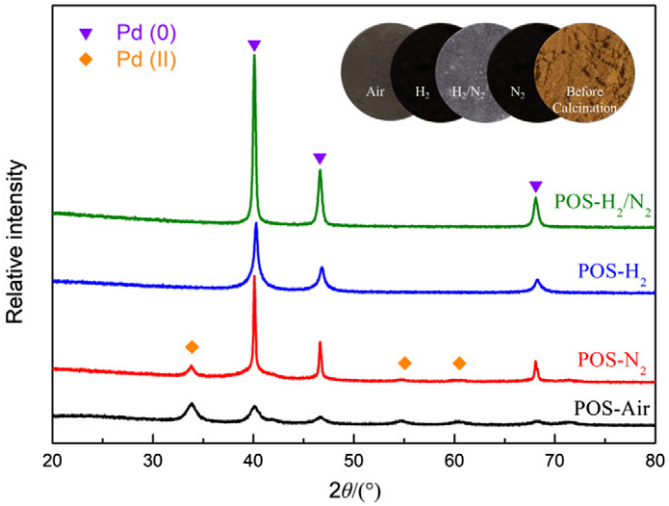

Fig. 4. XRD patterns of POS-Air, POS-N_2, POS-H_2 and POS-H_2/N_2 powders.

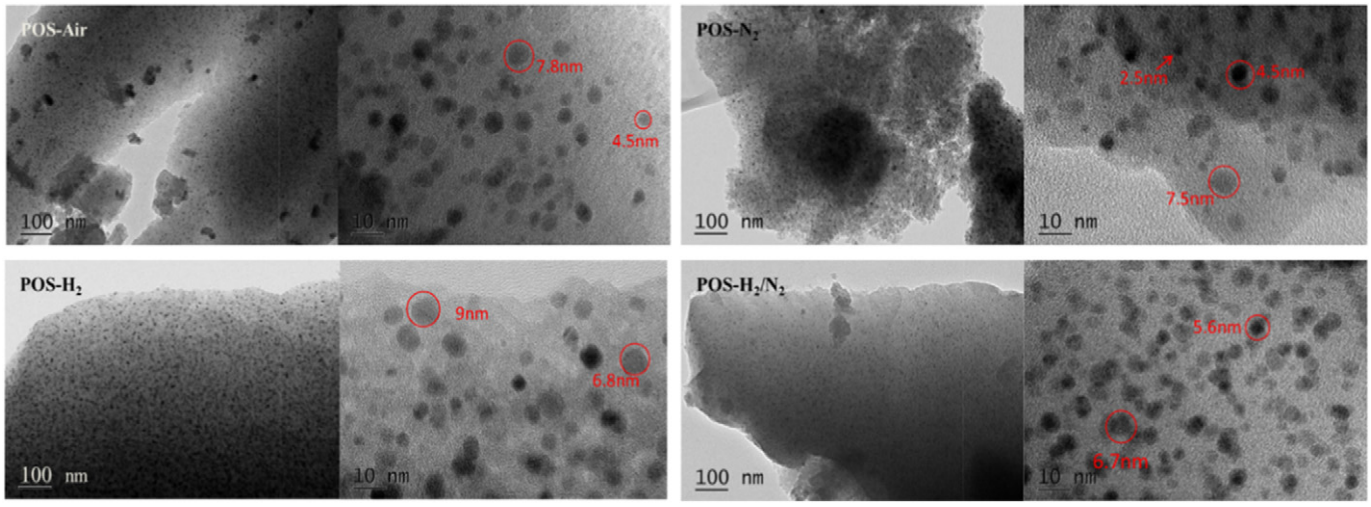

Fig. 5. TEM images of POS-Air, POS-N_2, POS-H_2 and POS-H_2/N_2 powders.

different atmospheres are disparate as well. The POS gel powders before further calcination are brown in color, while POS-Air and POS-H_2/N_2 powders are dark gray and gray-white, respectively. Moreover, POS-H_2 and POS-N_2 powders are close to black. The color differences between the four POS powders may indicate that the four POS powders have different chemical states or structures. In XRD patterns of the four powders, no diffraction peaks of crystalline SiO_2 were observed and Pd (0) characteristic peaks ($2\theta = 40.1°$, 46.7° and 68.2°) were detected corresponding to the (111), (200) and (220) plane reflections of palladium [36]. Pd (0) in POS-H_2 and POS-H_2/N_2 samples is easily understood due to the H_2 reduced reaction. However, the existence of characteristic peak of Pd (0) in POS-N_2 and POS-Air samples may be attributed to the heat treatment which was also found by Yang *et al.* [37]. In addition, the characteristic peaks at 34.2°, 54.5°, 60.2° and 71.5° represent the existence of Pd (II) in POS-N_2 and POS-Air powders. This is because $PdCl_2$ was used as palladium source and Pd (II) could be maintained under non-reductive calcination atmosphere.

Fig. 5 shows TEM images of the POS powders calcined at the four atmospheres. It can be observed from each case that Pd particles with a size range between 2 and 10 nm are randomly dispersed in an organosilica network, indicating that Pd has been successfully doped into the amorphous silica matrix. However, the distribution of Pd particles in the four cases is different. Many large aggregations were found from POS-Air sample under low magnification observation. The metal aggregation phenomenon may be attributed to the transformation of single Pd into PdO and the decomposition of ≡Si—CH_2—CH_2—Si≡ bonds [30]. Compared with the steric resistance

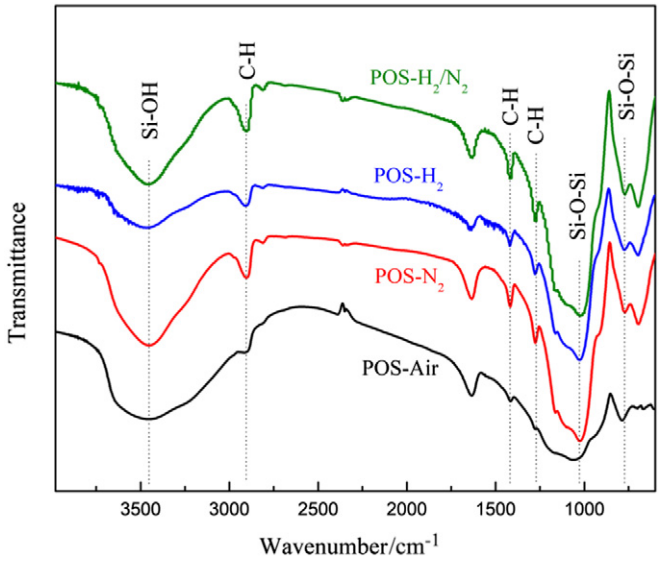

Fig. 6. FTIR spectra of POS-Air, POS-N_2, POS-H_2 and POS-H_2/N_2 powders.

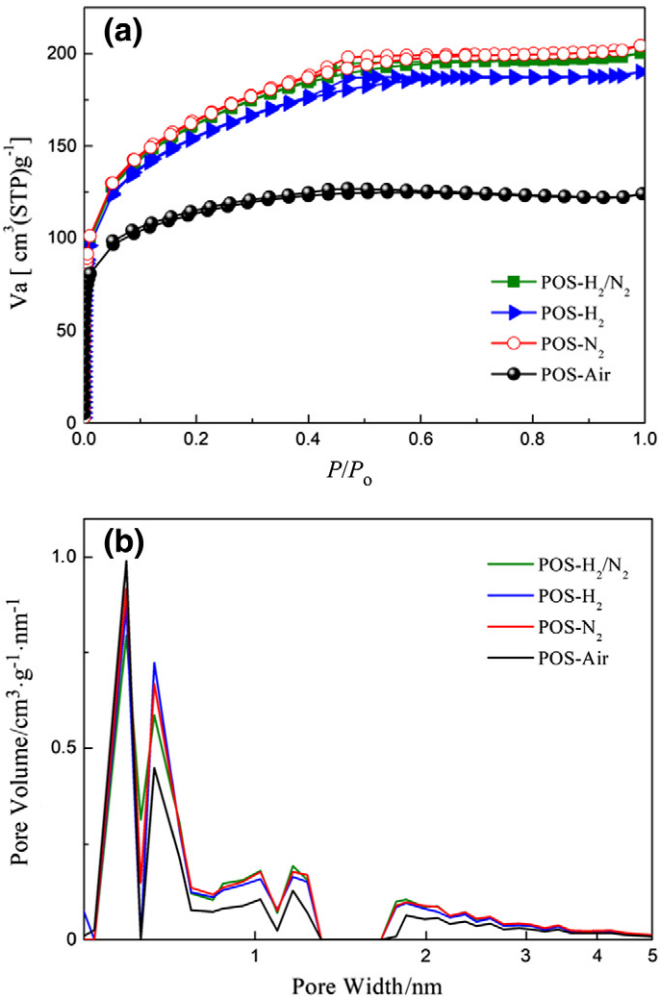

Fig. 7. (a) N_2 adsorption–desorption isotherms and (b) pore size distributions of POS-Air, POS-N_2, POS-H_2 and POS-H_2/N_2 powders.

Table 1
Pore structure data of POS-Air, POS-N_2, POS-H_2 and POS-H_2/N_2 powders

	$S_{BET}/m^2 \cdot g^{-1}$	$V_{total}/cm^3 \cdot g^{-1}$	$V_{micro}/cm^3 \cdot g^{-1}$	Average pore diameter/nm
POS-Air	410.18	0.19	0.64	0.87
POS-N_2	547.37	0.31	0.76	0.71
POS-H_2	507.18	0.29	0.77	0.71
POS-H_2/N_2	540.09	0.30	0.75	0.74

Note: S_{BET}, V_{total}, V_{micro} and average pore diameter represent Brunauer–Emmett–Teller (BET) specific surface area, total pore volume, micropore volume and microporosity, respectively.

Table 2
Permselectivities of POS-Air, POS-N_2, POS-H_2 and POS-H_2/N_2 membranes measured at 200 °C

	F_α (H_2/CO_2)	F_α (H_2/N_2)	F_α (H_2/CH_4)	F_α (H_2/SF_6)
POS-Air	8.91	10.4	8.4	21.7
POS-N_2	8.6	12.8	10.7	27.1
POS-H_2	8.0	29.3	31.3	1170
POS-H_2/N_2	15.0	96.7	173.0	3340

Note: F_α is permselectivity.

of Pd aggregation was reduced in POS-Air, Pd particles were uniformly dispersed in the other samples.

FTIR experiments were conducted to verify the chemical states of the four POS powder samples (Fig. 6). Characteristic peaks of POS samples at 3447, 2906, 1025 and 770 cm^{-1} correspond to Si—OH stretching vibration, C—H symmetric stretching vibrations, Si—O—Si asymmetric stretching vibrations, and Si—C stretching vibrations, respectively [38]. The co-existence of the shear vibration peak at 1274 cm^{-1} and the swing vibration peak at 1414 cm^{-1} is ascribed to ≡Si—CH_2—CH_2—Si≡ bond, which suggests the presence of organosilica segment in the samples [25]. It is obvious that the intensity of ≡Si—CH_2—CH_2—Si≡ bond in the POS-Air sample is the weakest in comparison with other POS powders calcined under inert or reducing gas atmosphere. Kanezashi *et al.* [39] also found that ≡Si—CH_2—CH_2—Si≡ bond may suffer from decomposition or carbonization when heated under air. Therefore, inert (N_2) and reducing (H_2, H_2/N_2) calcination atmosphere is more beneficial to maintain the organosilica moieties.

To investigate the effect of calcination atmosphere on the microstructure of POS membrane, N_2 adsorption–desorption experiments of POS powders calcined under the four atmospheres were conducted. Fig. 7a shows the N_2 adsorption–desorption curves of POS powders calcined under the four atmospheres. The type I N_2 adsorption isotherms of the four powders were found and all POS powder samples match with typical characteristics of microporous structure that extremely fast adsorption occurs at low pressure. The small hysteresis loops appeared at $P/P_0 = 0.45$ indicating that there is a certain amount of mesopores in the four POS powders. POS powders calcined under inert and reducing atmosphere exhibit similar N_2 adsorption capacity (about 180 cm^3 (STP)$\cdot g^{-1}$), while the N_2 adsorption capacity of POS-Air is much lower, only 125 cm^3 (STP)$\cdot g^{-1}$. The pore structure information derived from the N_2 adsorption–desorption results is given in Table 1. Similarly, specific surface area, total pore volume, average pore diameter and microporosity of POS powders calcined under inert and reducing atmosphere show nearly same values which are much different from those of POS-Air powder. Among the four samples, POS-Air powder has smaller specific surface area, total pore volume and average pore diameter but higher microporosity (0.87). The relatively small specific surface area and total pore volume of the POS-Air sample may be ascribed to the decomposition of organic chains that was determined by the aforementioned FTIR results. The consequent closure or collapse of pores leads to a denser structure of POS-Air membrane, in comparison with that of other POS membranes calcined under an inert or reducing atmosphere.

To further investigate pore size and its distribution of the as-prepared POS membranes, nonlocal density functional theory (NLDFT) model [40] analysis based on the N_2 adsorption–desorption curve was applied. In

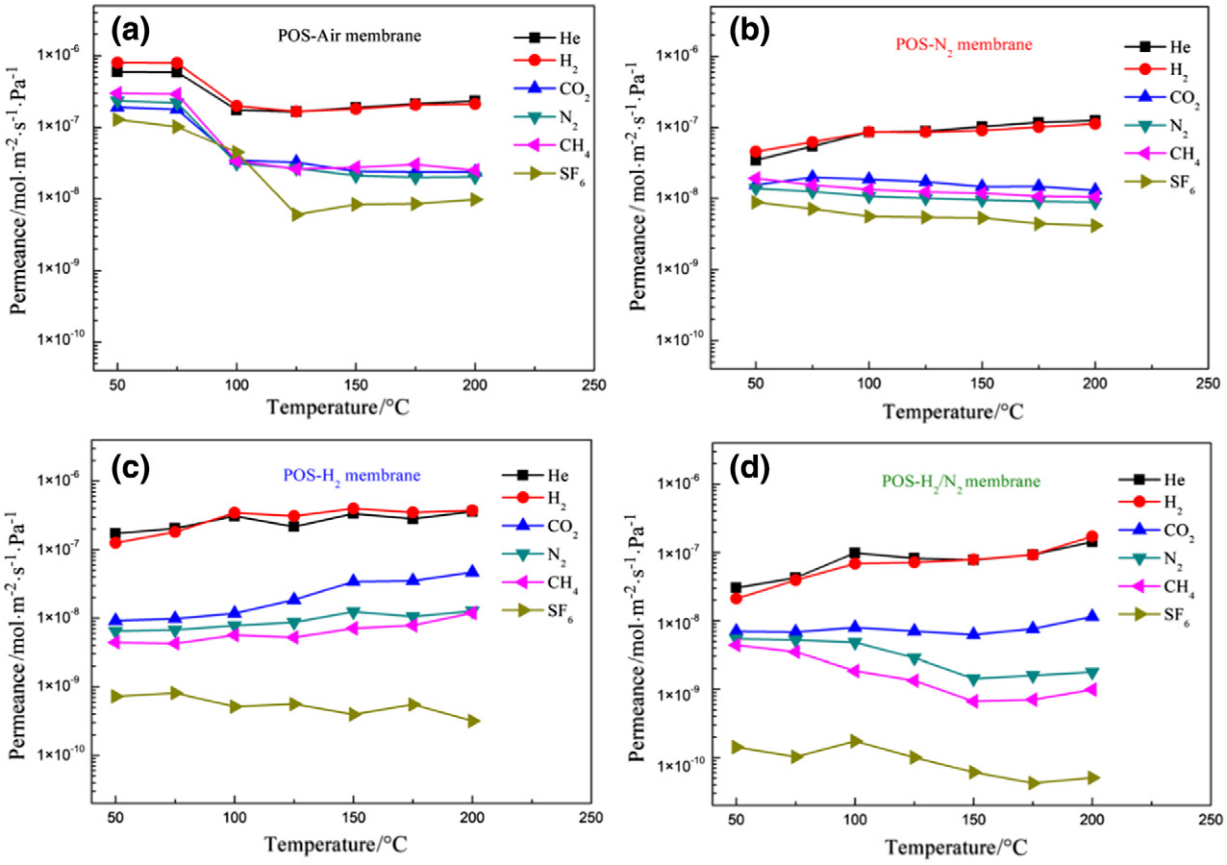

Fig. 8. Single-gas permeances of (a) POS-Air, (b) POS-N_2, (c) POS-H_2 and (d) POS-H_2/N_2 membranes tested under different temperatures.

Fig. 7b, the four POS powders have very similar multimodal pore size distribution and the pore size of the four samples is mainly distributed between 0.5 and 0.6 nm. A certain percent of mesopores with the pore size between 2 and 50 nm is found in each POS sample as well. It is observed that the POS-Air sample has a higher ratio of micropores and a lower ratio of mesopores compared with those of other POS samples.

3.3. Gas separation performance of POS membranes

3.3.1. Single-gas permeation

Single-gas permeances and permselectivities of the four POS membranes were studied at different temperatures ranging from 50 to 200 °C. In Fig. 8a, POS-Air membrane measured at 50 °C exhibits the highest permeance to all testing gases. This result may be caused by the formation of large pores or defects when calcined under air. H_2 and CO_2 permeance of the membrane measured at 50 °C are 8.01×10^{-7} and 1.91×10^{-7} mol·m^{-2}·s^{-1}·Pa^{-1}, respectively. When the testing temperature is above 100 °C, the gas permeances of POS-Air membrane showed a downward tendency to all gases. At 200 °C, H_2 and CO_2 permeance declined to 2.11×10^{-7} and 2.37×10^{-8} mol·m^{-2}·s^{-1}·Pa^{-1}, respectively. These results suggest that gas permeance of POS-Air membrane is not stable, which might be attributed to the fracture of the organic chain segment occurred during the calcination process under air atmosphere. Many small fragments (*e.g.* silanol groups) were generated during the calcination and moved by gas transport process to block micropores, resulting in gas permeance decline of POS-Air membrane [8].

In contrast, H_2 and He permeances of POS-N_2, POS-H_2 and POS-H_2/N_2 membranes slightly increase with the increase of temperature (Fig. 8b–d). The CO_2 permeance of the POS membrane calcined under inert atmosphere (*i.e.* POS-N_2) decreases slightly with the increase of the temperature, while CO_2 permeance of the POS membrane calcined under reducing atmosphere (*i.e.* POS-H_2 and POS-H_2/N_2) increases. This indicates that CO_2 passage through these POS membranes is based on different mechanisms. SF_6 molecules can permeate through the four POS membranes, which confirms the existence of mesopores in the membranes.

The four POS membranes measured at 200 °C exhibit good molecule sieving properties as the H_2 permselectivities of these membranes are much higher than the corresponding Knudsen diffusion factors and the results are compared in Table 2. Among the four membranes, POS-H_2/N_2 membrane shows the best H_2 separation performance that its permselectivities for H_2/CO_2, H_2/N_2, H_2/CH_4 and H_2/SF_6 are 15.0, 96.7, 173.0 and 3400.0, respectively. Tsuru [41] well established a simple intraparticle–interparticle pore model to explain gas permeation performance of silica membranes, and we also supplemented and confirmed it with a new experimental investigation [42]. Briefly, in organosilica network, internal pores (also known as intraparticle pores) are formed by a Si—O—Si and Si—CH_2—CH_2—Si hybrid structure and unconnected pores (also known as interparticle pores) are generated as voids between sol/gel particles. Small gas molecules (*e.g.* He and H_2) can permeate through intraparticle pores and interparticle pores, larger gas molecules (in kinetic diameter, *e.g.* CO_2, N_2, CH_4 and SF_6) may pass through organosilica membranes *via* interparticle pores. The mechanism is also applicable to explain the present study that calcination atmosphere can tailor the chemical state and porous structures of POS membranes for improving their permselectivities.

3.3.2. H_2 and CO_2 transport mechanism

Efficient separation of H_2 and CO_2 is of great importance for H_2 production in chemical industries. To further study H_2 and CO_2 transport mechanism through the as-prepared POS membranes, the relationship between gas permeance and temperature was studied. The gas permeance of the POS membranes can be calculated from Eq. 1 [43]:

$$F = F_0 \exp\left[\frac{-(E_a - E_{ads})}{RT}\right] = F_0 \exp\left(\frac{-\Delta E}{RT}\right) \quad (1)$$

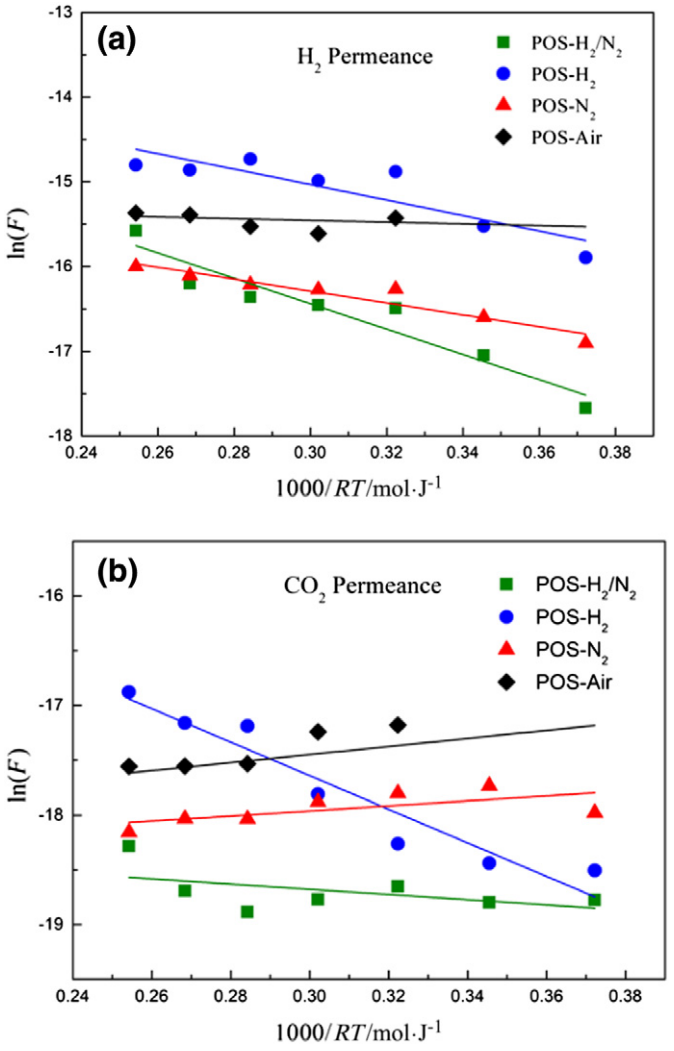

Fig. 9. Temperature dependency of (a) H_2 and (b) CO_2 permeances of POS-Air, POS-N_2, POS-H_2 and POS-H_2/N_2 membranes.

where F is gas permeance [mol·m^{-2}·s^{-1}·Pa^{-1}], F_0 the temperature independent parameter, R the gas constant [J·mol^{-1}·K^{-1}], T the absolute permeation temperature [K] and ΔE the apparent activation energy [J·mol^{-1}].

According to Eq. (1), the Arrhenius plots of H_2 and CO_2 permeances of the four membranes are shown in Fig. 9. The straight lines in the figures show linear fits to the data with slopes equal to $-\Delta E$ [kJ·mol^{-1}]. The positive ΔE suggests that a gas permeation through a membrane obeys the activated diffusion mechanism, while the negative ΔE suggests the process is mainly based on surface diffusion mechanism [44,45]. The apparent activation energies for H_2 and CO_2 permeation through the four POS membranes are presented in Table 3. The four apparent activation energy values for H_2 passage are positive, which implies that H_2 molecules pass through our membranes by activated diffusion. Higher activation energy means higher repulsive forces need to be overcome by gas molecules

Table 3
Apparent activation energy of H_2 and CO_2 through POS-Air, POS-N_2, POS-H_2 and POS-H_2/N_2 membranes

	ΔE_{H_2}/kJ·mol^{-1}	ΔE_{CO_2}/kJ·mol^{-1}
POS-Air	1.78	−6.36
POS-N_2	7.00	−2.27
POS-H_2	9.14	15.29
POS-H_2/N_2	14.96	2.37

Note: ΔE_{H_2} and ΔE_{CO_2} are the activation energy of H_2 and CO_2 pass through a membrane, respective.

through membrane pores. We found that the apparent activation energy for H_2 molecules passage through the POS-H_2/N_2 membrane is much higher than that of the POS-Air membrane. This may indicate that POS-Air membrane has a looser porous structure than that of POS-H_2/N_2 membrane owing to the differences in the POS networks formed under the different calcination atmospheres.

Notably, POS-H_2/N_2 and POS-H_2 membranes have positive apparent activation energies for CO_2 permeation, while POS-N_2 and POS-Air membranes have negative apparent activation energies for CO_2 permeation. This result suggests that the transport of the CO_2 molecules through POS-N_2 and POS-Air membrane is dominated by surface diffusion mechanism and the pores in the two membranes exhibited strong adsorption capacity to CO_2.

4. Conclusions

Four POS membranes calcined under different atmospheres were successfully prepared to investigate the effect of calcination atmosphere (*i.e.* air, N_2, H_2 and H_2/N_2) on gas separation performance of those membranes. A POS sol with a mean particle size of 7.53 nm was firstly synthesized for preparation of POS membranes. The TGA–DSC experiment of the POS gel was then conducted to confirm that calcination atmospheres have a significant effect on the chemical state and structure of the POS networks. XRD results confirm that Pd (II) could be only maintained under non-reductive calcination atmosphere (*i.e.* without H_2). FTIR analysis suggests that inert and reducing calcination atmosphere is more beneficial to keep organosilica moieties in POS networks. N_2 adsorption–desorption experiments indicate that the pore size of the four membranes is mainly distributed between 0.5 and 0.6 nm with the existence of a certain amount of mesopores.

For gas separation performance, all four POS membranes measured at 200 °C exhibit good permeance to small gas molecules (*i.e.* He and H_2) and the H_2 permselectivities of these membranes are much higher than the corresponding Knudsen diffusion factors. Among the four membranes, POS-H_2/N_2 membrane shows the optimal H_2 separation performance that its permselectivities for H_2/CO_2, H_2/N_2, H_2/CH_4 and H_2/SF_6 are 15.0, 96.7, 173.0 and 3400.0, respectively. In addition, the analysis of activation energies points out that H_2 molecules pass through the four membranes by activated diffusion, while CO_2 molecule permeation through POS-N_2 and POS-Air membrane is dominated by surface diffusion.

References

[1] A.J. Burgraff, L. Cot, Fundamentals of Inorganic Membrane Science and Technology, Elsevier, 1996.
[2] L. Cot, C. Guizard, A. Julbe, A. L, Preparation and Application of Inorganic Membranes, Springer, Dordrecht, 1994.
[3] S.M. Samaei, S. Gato-Trinidad, A. Altaee, The application of pressure-driven ceramic membrane technology for the treatment of industrial wastewaters — A review, *Sep. Purif. Technol.* 200 (2018) 198–220.
[4] J.Y.S. Lin, L. Winnubst, Letter to the editor, *J. Membr. Sci.* (2017) 542.
[5] R.J.R. Uhlhorn, M.H.B.J. Huis In't Veld, K. Keizer, A.J. Burggraaf, High permselectivities of microporous silica-modified γ-alumina membranes, *J. Mater. Sci. Lett.* 8 (1989) 1135–1138.
[6] R.M. de Vos, H. Verweij, High-selectivity, high-flux silica membranes for gas separation, *Science* 279 (1998) 1710–1711.
[7] M. ten Hove, M.W.J. Luiten-Olieman, C. Huiskes, A. Nijmeijer, L. Winnubst, Hydrothermal stability of silica, hybrid silica and Zr-doped hybrid silica membranes, *Sep. Purif. Technol.* 189 (2017) 48–53.
[8] M.C. Duke, J.C.D. da Costa, D.D. Do, P.G. Gray, G.Q. Lu, Hydrothermally robust molecular sieve silica for wet gas separation, *Adv. Funct. Mater.* 16 (2006) 1215–1220.
[9] H.L. Castricum, A. Sah, R. Kreiter, D.H. Blank, J.F. Vente, J.E. ten Elshof, Hybrid ceramic nanosieves: Stabilizing nanopores with organic links, *Chem. Commun. (Camb)* (2008) 1103–1105.
[10] M. Kanezashi, K. Yada, T. Yoshioka, T. Tsuru, Design of silica networks for development of highly permeable hydrogen separation membranes with hydrothermal stability, *J. Am. Chem. Soc.* 131 (2009) 414–415.
[11] J. Wang, M. Kanezashi, T. Yoshioka, T. Tsuru, Effect of calcination temperature on the PV dehydration performance of alcohol aqueous solutions through BTESE-derived silica membranes, *J. Membr. Sci.* 415-416 (2012) 810–815.
[12] A.P. Dral, K. Tempelman, E.J. Kappert, L. Winnubst, N.E. Benes, J.E. ten Elshof, Long-term flexibility-based structural evolution and condensation in microporous organosilica membranes for gas separation, *J. Mater. Chem. A* 5 (2017) 1268–1281.
[13] K. Yamamoto, J. Ohshita, T. Mizumo, M. Kanezashi, T. Tsuru, Synthesis of organically bridged trialkoxysilanes bearing acetoxymethyl groups and applications to reverse osmosis membranes, *Appl. Organomet. Chem.* 31 (2017).
[14] H. Qi, Preparation of composite microporous silica membranes using TEOS and 1, 2-bis(triethoxysilyl)ethane as precursors for gas separation, *Chin. J. Chem. Eng.* 19 (2011) 404–409.
[15] H. Qi, J. Han, N. Xu, H.J. Bouwmeester, Hybrid organic–inorganic microporous membranes with high hydrothermal stability for the separation of carbon dioxide, *ChemSusChem* 3 (2010) 1375–1378.
[16] K.-S. Chang, T. Yoshioka, M. Kanezashi, T. Tsuru, K.-L. Tung, Molecular simulation of micro-structures and gas diffusion behavior of organic–inorganic hybrid amorphous silica membranes, *J. Membr. Sci.* 381 (2011) 90–101.
[17] H.L. Castricum, G.G. Paradis, M.C. Mittelmeijer-Hazeleger, R. Kreiter, J.F. Vente, J.E. ten Elshof, Tailoring the separation behavior of hybrid organosilica membranes by adjusting the structure of the organic bridging group, *Adv. Funct. Mater.* 21 (2011) 2319–2329.
[18] Y.S. Lin, Microporous and dense inorganic membranes: Current status and prospective, *Sep. Purif. Technol.* 25 (2001) 39–55.
[19] H. Song, Y. Wei, C. Wang, S. Zhao, H. Qi, Tuning sol size to optimize organosilica membranes for gas separation, *Chin. J. Chem. Eng.* 26 (2018) 53–59.
[20] H. Qi, J. Han, N. Xu, Effect of calcination temperature on carbon dioxide separation properties of a novel microporous hybrid silica membrane, *J. Membr. Sci.* 382 (2011) 231–237.
[21] E.J. Kappert, H.J. Bouwmeester, N.E. Benes, A. Nijmeijer, Kinetic analysis of the thermal processing of silica and organosilica, *J. Phys. Chem. B* 118 (2014) 5270–5277.
[22] M. ten Hove, A. Nijmeijer, L. Winnubst, Facile synthesis of zirconia doped hybrid organic inorganic silica membranes, *Sep. Purif. Technol.* 147 (2015) 372–378.
[23] H.L. Castricum, H.F. Qureshi, A. Nijmeijer, L. Winnubst, Hybrid silica membranes with enhanced hydrogen and CO_2 separation properties, *J. Membr. Sci.* 488 (2015) 121–128.
[24] H.F. Qureshi, A. Nijmeijer, L. Winnubst, Influence of sol–gel process parameters on the micro-structure and performance of hybrid silica membranes, *J. Membr. Sci.* 446 (2013) 19–25.
[25] H.F. Qureshi, R. Besselink, J.E. ten Elshof, A. Nijmeijer, L. Winnubst, Doped microporous hybrid silica membranes for gas separation, *J. Sol-Gel Sci. Technol.* 75 (2015) 180–188.
[26] H. Qi, H. Chen, L. Li, G. Zhu, N. Xu, Effect of Nb content on hydrothermal stability of a novel ethylene-bridged silsesquioxane molecular sieving membrane for H_2/CO_2 separation, *J. Membr. Sci.* 421-422 (2012) 190–200.
[27] H. Song, S. Zhao, J. Chen, H. Qi, Hydrothermally stable Zr-doped organosilica membranes for H_2/CO_2 separation, *Microporous Mesoporous Mater.* 224 (2016) 277–284.
[28] P. Karakiliç, C. Huiskes, M.W.J. Luiten-Olieman, A. Nijmeijer, L. Winnubst, Sol–gel processed magnesium-doped silica membranes with improved H_2/CO_2 separation, *J. Membr. Sci.* 543 (2017) 195–201.
[29] David Uhlmann, Bradley P. Ladewig Shaomin, João C. Diniz da Costa, Cobalt-doped silica membranes for gas separation, *J. Membr. Sci.* 326 (2009) 316–321.
[30] M. Kanezashi, D. Fuchigami, T. Yoshioka, T. Tsuru, Control of Pd dispersion in sol–gel-derived amorphous silica membranes for hydrogen separation at high temperatures, *J. Membr. Sci.* 439 (2013) 78–86.
[31] B. Ballinger, J. Motuzas, S. Smart, J.C.D. da Costa, Palladium cobalt binary doping of molecular sieving silica membranes, *J. Membr. Sci.* 451 (2014) 185–191.
[32] H. Song, S. Zhao, J. Lei, C. Wang, H. Qi, Pd-doped organosilica membrane with enhanced gas permeability and hydrothermal stability for gas separation, *J. Mater. Sci.* 51 (2016) 6275–6286.
[33] J. Lei, H. Song, Y. Wei, S. Zhao, H. Qi, A novel strategy to enhance hydrothermal stability of Pd-doped organosilica membrane for hydrogen separation, *Microporous Mesoporous Mater.* 253 (2017) 55–63.
[34] Y. Chua, C.X.C. Lin, F. Kleitz, S. Smart, Mesoporous organosilica membranes: Effects of pore geometry and calcination conditions on the membrane distillation performance for desalination, *Desalination* 370 (2015) 53–62.
[35] H.R. Lee, T. Shibata, M. Kanezashi, T. Mizumo, J. Ohshita, T. Tsuru, Pore-size-controlled silica membranes with disiloxane alkoxides for gas separation, *J. Membr. Sci.* 383 (2011) 152–158.
[36] D.-T. Phan, G.-S. Chung, Characteristics of resistivity-type hydrogen sensing based on palladium–graphene nanocomposites, *Int. J. Hydrog. Energy* 39 (2014) 620–629.
[37] Y. Jing, F. Wangqing, B. Carl-Martin, Effect of calcination atmosphere on microstructure and H_2/CO_2 separation of palladium-doped silica membranes, *Sep. Purif. Technol.* 210 (2019) 659–669.
[38] K. Yamamoto, J. Ohshita, T. Mizumo, T. Tsuru, Efficient synthesis of SiOC glasses from ethane, ethylene, and acetylene-bridged polysilsesquioxanes, *J. Non-Cryst. Solids* 408 (2015) 137–141.
[39] M. Kanezashi, K. Yada, T. Yoshioka, T. Tsuru, Organic–inorganic hybrid silica membranes with controlled silica network size: Preparation and gas permeation characteristics, *J. Membr. Sci.* 348 (2010) 310–318.
[40] M.M. Wei, L. Zhang, Y.Q. Xiong, J.H. Li, P.A. Peng, Nanopore structure characterization for organic-rich shale using the non-local-density functional theory by a combination of N_2 and CO_2 adsorption, *Microporous Mesoporous Mater.* 227 (2016) 88–94.
[41] T. Tsuru, Nano/subnano-tuning of porous ceramic membranes for molecular separation, *J. Sol-Gel Sci. Technol.* 46 (2008) 349–361.
[42] H. Song, Y. Wei, H. Qi, Tailoring pore structures to improve the permselectivity of organosilica membranes by tuning calcination parameters, *J. Mater. Chem. A* 5 (2017) 24657–24666.
[43] V. Boffa, D. Blank, J. Tenelshof, Hydrothermal stability of microporous silica and niobia–silica membranes, *J. Membr. Sci.* 319 (2008) 256–263.
[44] T. Yoshioka, E. Nakanishi, T. Tsuru, M. Asaeda, Experimental studies of gas permeation through microporous silica membranes, *AIChE J.* 47 (2001) 2052–2063.
[45] H. Nagasawa, T. Niimi, M. Kanezashi, T. Yoshioka, T. Tsuru, Modified gas-translation model for prediction of gas permeation through microporous organosilica membranes, *AIChE J.* 60 (2014) 4199–4210.